Temperature-dependent coherent carrier transport in quantum cascade lasers

2011 New J. Phys. 13 083027

(http://iopscience.iop.org/1367-2630/13/8/083027)

New Journal of Physics
The open-access journal for physics

Temperature-dependent coherent carrier transport in quantum cascade lasers

Muhammad Anisuzzaman Talukder[1,2] **and Curtis R Menyuk**
Department of Computer Science and Electrical Engineering, University of Maryland, Baltimore County, 1000 Hilltop Circle, Baltimore, MD 21250, USA
E-mail: anisuzzaman@umbc.edu

New Journal of Physics **13** (2011) 083027 (12pp)
Received 29 September 2010
Published 24 August 2011
Online at http://www.njp.org/
doi:10.1088/1367-2630/13/8/083027

Abstract. The temperature dependence of coherent carrier transport in quantum cascade lasers (QCLs) is studied in this paper. It was found that coherent carrier transport in QCLs decreases as the temperature increases because the coherence between the injector and active region energy levels decays at a faster rate with increasing temperature. Calculations show that the coherence time decreases by at least a factor of two as the temperature increases from 100 K to room temperature. Electron transport from the injector regions into the active regions and vice versa is a highly coherent process that becomes less efficient with decreasing coherence time and hence becomes less efficient with increasing temperature. As a consequence, when the temperature increases, the population of the upper lasing levels in active regions decreases, the population of the lower lasing levels increases and performance suffers.

Contents

[1] Current address: Department of Electrical and Electronic Engineering, Bangladesh University of Engineering and Technology, Dhaka 1000, Bangladesh.
[2] Author to whom any correspondence should be addressed.

1. Introduction

The carrier dynamics of quantum cascade lasers (QCLs) is responsible for the overall performance in many ways. Calculation of the carrier dynamics is key to understanding the underlying physics and designing an optimum structure for improved performance, but the carrier dynamics of QCLs is complicated. Several different incoherent scattering processes and coherent tunneling are responsible for the electron transport between the quantized energy levels [1–5]. In a typical QCL structure, scattering is principally responsible for transport within an injector region and within an active region, while coherent tunneling is principally responsible for carrier transport between an injector and an active region.

In practice, it is desirable to operate QCLs at room temperature at the highest power that can be obtained. The highest power level that has been obtained in practice is 3.4 W operating continuous wave at room temperature [6]. It has been observed that a QCL's performance drops dramatically when the temperature rises [6]. This performance drop is usually attributed to the scattering of electrons from the injector levels and the upper lasing level to levels that are not localized within the conduction band, leading to a decrease in the number of electrons that take part in the lasing process [7]. Additionally, electrons may scatter back to the lower lasing level of the preceding active region from injector levels—a process that is referred to as back-filling [7]. The temperature-dependent performance drop may also be due to the decrease in the upper lasing level lifetime at a higher temperature, especially in the case of THz QCLs. All of these processes reduce the population inversion and hence the gain. However, the electrons that scatter to non-localized, quasi-continuum levels may scatter down to levels that are localized within the conduction band and contribute to the radiative process at a later stage. Improved designs are being used to reduce losses due to these effects. To reduce the scattering to quasi-continuum levels, injector and active region levels are designed to be well within the barrier potential height. Quasi-continuum energy levels are designed to be separated by at least 3–5 times the LO phonon energy from the upper lasing level [7]. The injector regions are designed to act as Bragg reflectors for the upper lasing level in the preceding active regions so that electrons cannot escape [8]. A highly strained InGaAs/InAlAs material system is used to make the quantum wells deeper [9, 10]. Additionally, materials with a higher-energy offset, e.g. AlAs, are being used as the exit barrier [11]. Back-scattering is reduced by increasing the energy separation between the lower lasing level and the injector levels, especially the injector ground level [7]. However, even with these design improvements, performance degradation due to temperature increases remains a serious problem. The improvement in performance has been lower than the calculations would suggest.

In this paper, we will show that in addition to the loss of electrons due to scattering into the quasi-continuum energy levels and back-filling, increasingly inefficient coherent transport is also responsible for the drop in QCL performance as the temperature rises. Carrier injection into the upper lasing level and extraction from the lower lasing level are largely due to coherent tunneling, whose efficiency depends on the coherence time. The coherence time diminishes as the temperature increases.

To carry out this study, we use a density matrix transport model that is similar to the one described by Terazzi and Faist [12]. This model assumes a Maxwellian momentum distribution in the two spatial dimensions that are transverse to the quantum wells, which allows us to explicitly calculate the scattering cross sections. This approach is less accurate than Monte Carlo or full quantum mechanical simulations [5, 13, 14], but it is sufficiently accurate for

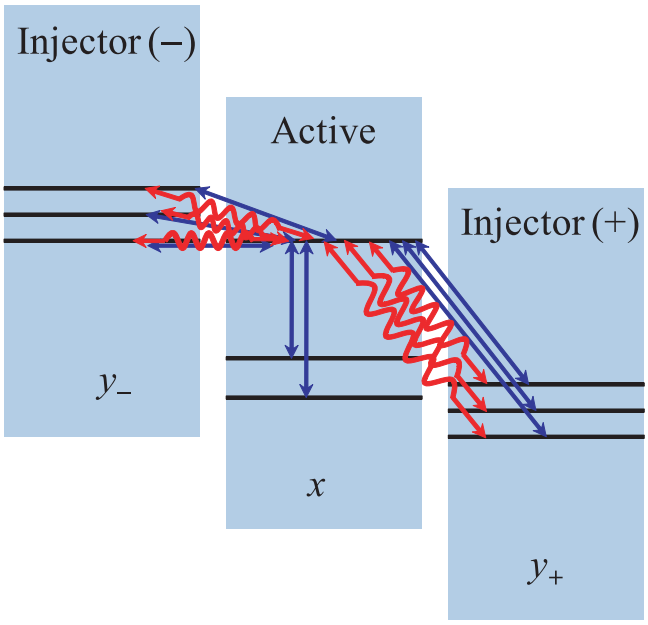

Figure 1. Schematic illustration of the carrier transport model. We show how the carrier density of the upper lasing level is related to other levels in the system. The blue straight arrows represent incoherent scattering mechanisms. The red wavy arrows indicate coherent carrier transport. We use double arrows for both incoherent and coherent mechanisms to signify that the carrier transport can be in either direction. Here we show three levels in each active and injector region. However, the carrier density formulation of a level remains the same irrespective of the number of levels in any region and the relative energy spacing of other levels.

our purposes and is computationally rapid enough to allow us to study structures with realistic geometries. At the same time, it is more accurate than the widely used models that solve the rate equations [15–18]. The rate equations are useful in designing QCL structures, but they do not take into account quantum coherence between the energy levels. Quantum coherence often plays a crucial role in QCLs. In particular, as we will show in this study, it is of critical importance for understanding how temperature affects the carrier transport.

The remainder of this paper is organized as follows. In section 2, we present the density matrix equations and discuss the carrier transport model. In particular, we describe how quantum coherence effects should be included in the model. In section 3, we present the results of our QCL transport model. We present and discuss the change in time evolution of the carrier densities and in coherence as the temperature varies. In section 4, the results are summarized and the conclusions are presented.

2. The theoretical model

We write the density matrix equations in a way that includes both the incoherent scattering and coherent tunneling mechanisms [13, 15–21]. In figure 1, we show a schematic illustration of how the carrier density matrix equations are formulated in our model. The density matrix

equations are

$$\frac{\mathrm{d}n_{\mathrm{A},x}}{\mathrm{d}t} = \sum_{x'\neq x}\frac{n_{\mathrm{A},x'}}{s_{x'x}} + \sum_{y_-}\frac{n_{\mathrm{I},y-}}{s_{y_-x}} + \sum_{y_+}\frac{n_{\mathrm{I},y+}}{s_{y_+x}} - \sum_{y_-}\frac{n_{\mathrm{A},x}}{s_{xy_-}} - \sum_{x'\neq x}\frac{n_{\mathrm{A},x}}{s_{xx'}} - \sum_{y_+}\frac{n_{\mathrm{A},x}}{s_{xy_+}} - \mathrm{i}\sum_{y_+}\frac{\Delta_{0,xy_+}}{2\hbar}(C_{xy_+} - C^*_{xy_+}) + \mathrm{i}\sum_{y_-}\frac{\Delta_{0,y_-x}}{2\hbar}(C_{y_-x} - C^*_{y_-x}), \tag{1a}$$

$$\frac{\mathrm{d}n_{\mathrm{I},y-}}{\mathrm{d}t} = \sum_{y'_-\neq y_-}\frac{n_{\mathrm{I},y'_-}}{s_{y'_-y_-}} + \sum_{x}\frac{n_{\mathrm{A},x}}{s_{xy_+}} + \sum_{x}\frac{n_{\mathrm{A},x}}{s_{xy_-}} - \sum_{x}\frac{n_{\mathrm{I},y_-}}{s_{y_-x}} - \sum_{x}\frac{n_{\mathrm{I},y_+}}{s_{y_+x}} - \sum_{y'_-\neq y_-}\frac{n_{\mathrm{I},y_-}}{s_{y_-y'_-}} - \mathrm{i}\sum_{x}\frac{\Delta_{0,y_-x}}{2\hbar}(C_{y_-x} - C^*_{y_-x}) + \mathrm{i}\sum_{x}\frac{\Delta_{0,xy_+}}{2\hbar}(C_{xy_+} - C^*_{xy_+}), \tag{1b}$$

$$\frac{\mathrm{d}n_{\mathrm{I},y+}}{\mathrm{d}t} = \sum_{y'_+\neq y_+}\frac{n_{\mathrm{I},y'_+}}{s_{y'_+y_+}} + \sum_{x}\frac{n_{\mathrm{A},x}}{s_{xy_+}} + \sum_{x}\frac{n_{\mathrm{A},x}}{s_{xy_-}} - \sum_{y'_+\neq y_+}\frac{n_{\mathrm{I},y_+}}{s_{y_+y'_+}} - \sum_{x}\frac{n_{\mathrm{I},y_+}}{s_{y_+x}} - \sum_{x}\frac{n_{\mathrm{I},y_-}}{s_{y_-x}} - \mathrm{i}\sum_{x}\frac{\Delta_{0,y_-x}}{2\hbar}(C_{y_-x} - C^*_{y_-x}) + \mathrm{i}\sum_{x}\frac{\Delta_{0,xy_+}}{2\hbar}(C_{xy_+} - C^*_{xy_+}), \tag{1c}$$

$$\frac{\mathrm{d}C_{xy_+}}{\mathrm{d}t} = \mathrm{i}\frac{\Delta_{0,xy_+}}{2\hbar}(n_{\mathrm{I},y_+} - n_{\mathrm{A},x}) - \frac{C_{xy_+}}{T_{2,xy_+}} - \mathrm{i}\frac{E_{xy_+}}{\hbar}C_{xy_+}, \tag{1d}$$

$$\frac{\mathrm{d}C_{y_-x}}{\mathrm{d}t} = \mathrm{i}\frac{\Delta_{0,y_-x}}{2\hbar}(n_{\mathrm{A},x} - n_{\mathrm{I},y_-}) - \frac{C_{y_-x}}{T_{2,y_-x}} - \mathrm{i}\frac{E_{y_-x}}{\hbar}C_{y_-x}. \tag{1e}$$

In this formulation of the density matrix equations, we have taken one active region and two injector regions preceding and following the active region. In QCLs, each active and injector region will have several levels. The summations in equation (1) include all the levels of the active and injector regions. This model can be extended to include additional periods. In the cases we investigated, we found that this number of periods is adequate to ensure the accuracy of the results [22]. In equation (1), the parameter n is the carrier density in the energy levels. Subscripts A and I denote active and injector regions, respectively. Indices x and y indicate the levels in the active and injector regions, respectively. Subscripts $-$ and $+$ denote a quantity in the injector region that precedes and follows the active region, respectively. The parameter C_{xy} is the coherence between levels x and y. The parameter s_{xy} is the scattering time between levels x and y. The parameter $\Delta_{0,xy}$ is the energy splitting at resonance between levels x and y, whereas E_{xy} is the detuning of the energy of level x (E_x) and the energy of level y (E_y) from resonance. The parameter $T_{2,xy}$ is the coherence time between levels x and y.

The scattering time s_{xy} is determined mainly by electron–LO-phonon and electron–electron scattering. Electron–LO-phonon scattering dominates in intersubband transitions [23, 24], but electron–electron scattering becomes important when the energy spacing between the levels is smaller than the LO-phonon resonance, so that LO-phonon scattering is forbidden except for the electrons in the high-energy tail [15]. Electron–electron scattering dominates in intrasubband transitions [25].

If two energy levels of two neighboring quantum wells that are separated by a potential barrier coherently couple, electron wave packets can propagate or tunnel through the barrier from one energy level to another [26, 27]. Before achieving their steady-state values, electron wave packets oscillate between the levels in what are referred to as Rabi oscillations. The coherent transport depends on the strength of the coherence, the detuning of the levels from resonance and the lifetime of the coherence. The strength of the coherence depends on the energy splitting of the levels at resonance ($\Delta_{0,xy}$), which in turn depends on the thickness and height of the barrier between neighboring quantum wells [1, 28]. As the thickness of the barrier or the height of the barrier increases, the coherence between the levels decreases. The barrier thickness is a design parameter, whereas the barrier height depends on the choice of the material system. Since in QCLs electron tunneling is most important from the injector ground level to the upper lasing level and those two levels are in two neighboring quantum wells separated by the injection barrier, selection of the thickness of the injection barrier has a significant role in determining the tunneling transport. The detuning of the levels from resonance (E_{xy}) depends on the applied electric field. When there is no detuning, i.e. $E_{xy} = 0$, coherent carrier transport reaches its peak.

While propagating, electronic wave packets lose phase coherence mainly due to intra-subband scattering by LO phonons, coulombic potential from other electrons in the subband and roughness in the interfaces of well and barrier materials [29, 30]. These scattering times depend on the quantum mechanical design, quality of the interfaces during the growth of the heterostructure, carrier density and temperature. Therefore, so does the coherence time. Once the QCL is designed and grown, the coherence time depends mainly on the temperature. Hence, in a fixed electric field, the coherent carrier transport will also depend mainly on the temperature.

The coherence time $T_{2,xy}$ between levels x and y can be written as

$$\frac{1}{T_{2,xy}} = \frac{1}{T_{2,xy}^{\text{electron}}} + \frac{1}{T_{2,xy}^{\text{phonon}}} + \frac{1}{T_{2,xy}^{\text{roughness}}}, \tag{2}$$

where $T_{2,xy}^{\text{electron}}$, $T_{2,xy}^{\text{phonon}}$ and $T_{2,xy}^{\text{roughness}}$ are the contributions to the coherence time $T_{2,xy}$ due to electron–electron scattering, electron–LO-phonon scattering, and electron–interface roughness scattering, respectively. The propagating electrons may lose phase coherence either in level x or in level y. The scattering of an electron in subband x due to an electron or an LO phonon is uncorrelated with the scattering of an electron in subband y due to an electron or an LO phonon. Therefore, intrasubband electron–electron and electron–LO-phonon transitions in levels x and y separately contribute to the loss of phase coherence and the rates add linearly. In the calculations presented here, we consider the dominant intrasubband electron–electron transitions, i.e. $x, x \to x, x$ and $y, y \to y, y$, where $x, x \to x, x$ denotes two electrons that are initially in subband x and subsequently scatter into the same subband. In order to reduce the computational burden, we typically neglect the less significant intrasubband electron–electron scattering, such as $x, y \to x, y$, where $x, y \to x, y$ denotes two electrons that are initially in different subbands x and y and subsequently scatter into the same two subbands. However, we have seen that the results do not change by a significant amount when $x, y \to x, y$ scattering is included in the model. Therefore, we write the contribution of the electron–electron scattering to the coherence time as

$$\frac{1}{T_{2,xy}^{\text{electron}}} = \frac{1}{s_{x,x\to x,x}^{\text{electron}}} + \frac{1}{s_{y,y\to y,y}^{\text{electron}}}, \tag{3}$$

where $s^{\text{electron}}_{x,x\to x,x}$ is the scattering lifetime due to $x, x \to x, x$ electron–electron transitions. For electron–LO-phonon scattering, an electron may scatter by emitting an LO phonon or by absorbing an LO phonon. Although electron scattering due to LO-phonon absorption is not significant in intersubband transitions, it is as significant as scattering due to LO-phonon emission in intrasubband transitions [31]. Hence, scattering due to both LO-phonon emission and LO-phonon absorption in both x and y levels should be included to calculate $T_{2,xy}$. Therefore, we write

$$\frac{1}{T^{\text{phonon}}_{2,xy}} = \frac{1}{s^{\text{phonon,abs}}_{x\to x}} + \frac{1}{s^{\text{phonon,em}}_{x\to x}} + \frac{1}{s^{\text{phonon,abs}}_{y\to y}} + \frac{1}{s^{\text{phonon,em}}_{y\to y}}, \tag{4}$$

where $s^{\text{phonon}}_{x\to x}$ is the scattering lifetime due to $x \to x$ electron–LO-phonon transitions and the superscripts 'abs' and 'em' denote absorption and emission, respectively. The intrasubband scattering due to interface roughness in levels x and y is correlated. Non-uniformity in a surface between two alternating materials causes a change in the energy of all the electrons that have a finite probability of existence near that interface. Therefore, the intrasubband scattering rate in level x and the intrasubband scattering rate in level y due to interface roughness cannot be linearly added when calculating the coherence time. Instead, we write [30, 32]

$$\frac{1}{T^{\text{roughness}}_{2,xy}} = \frac{1}{s^{\text{roughness}}_{x\to x}} + \frac{1}{s^{\text{roughness}}_{y\to y}} - 2\,\frac{1}{\sqrt{s^{\text{roughness}}_{x\to x}\, s^{\text{roughness}}_{y\to y}}}, \tag{5}$$

where $s^{\text{roughness}}_{x\to x}$ is the scattering lifetime due to $x \to x$ electron–interface roughness transitions.

The resonance energy splitting $\Delta_{0,xy}$ is calculated by applying a variable electric field and determining the minimum energy spacings between any two energy levels. The electron–LO-phonon and electron–electron scattering rates are calculated using the approach that is discussed in [33], and the electron–interface roughness scattering rate is calculated using the approach that is discussed in [32].

3. Results

We implement this transport model for the QCL structure of [34]. A similar structure has been used by Woerner *et al* [29] for their pump–probe experiments. This particular QCL is designed using a GaAs/AlGaAs material system and emits at a mid-infrared (mid-IR) wavelength. The quantum mechanical design of the QCL is typical of mid-IR QCLs. Therefore, the results presented in this study should qualitatively apply to any QCL that emits at a mid-IR wavelength. In particular, we have also performed similar calculations for the mid-IR QCL of [35], which is designed using an InGaAs/InAlAs material system, and we obtained similar results. The conduction band potential edge profile and the corresponding moduli-squared wavefunctions of this QCL have been plotted in figure 2. Levels 1–3 are in the active region and levels 4–8 are in the injector.

We calculate the time-resolved solutions of equations (1*a*)–(1*e*), so that transient carrier transport phenomena can be visualized and the underlying physics can be explained. Initially, we distribute all the carriers of a period to the injector levels only. Therefore, at the start of our computational solution, all the active region levels are empty. With time, the carrier density in each level changes. As the parameters s_{xy} and $T_{2,xy}$ depend on the carrier densities in levels x and y, we recalculate these parameters as the carriers evolve and until the carriers reach their steady-state values.

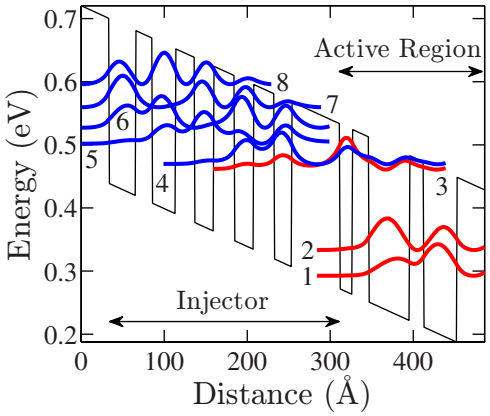

Figure 2. Conduction band diagram and moduli-squared wavefunctions of the QCL of [34]. The applied electric field is 60 kV cm^{-1}.

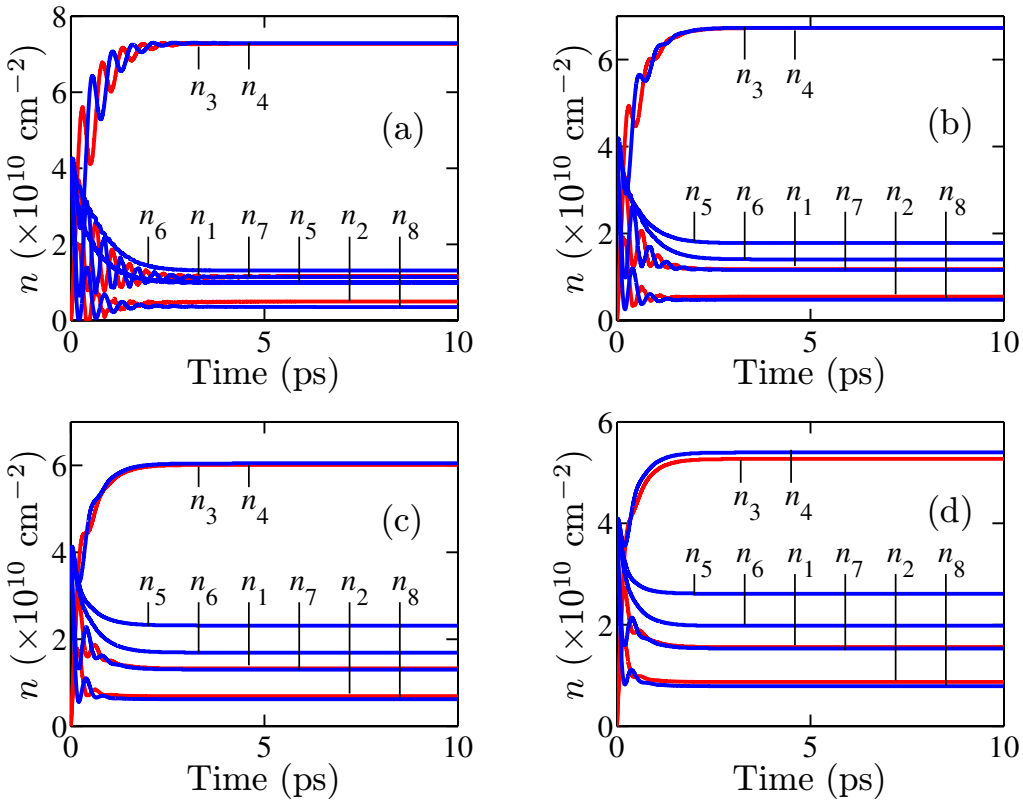

Figure 3. Time evolution of carrier density at different levels in the QCL of Sirtori *et al* [34]. The applied electric field is 60 kV cm^{-1}, and the total carrier density per period is 2×10^{11} cm^{-2}. The temperature is (a) $T = 100$ K, (b) $T = 200$ K, (c) $T = 300$ K and (d) $T = 400$ K.

We present in figure 3 the time evolution of the carrier density at each level of the QCL structure with a temperature of (a) 100 K, (b) 200 K, (c) 300 K and (d) 400 K. The total number of carriers (N_d) in each period is 2×10^{11} cm^{-2} and the QCL is biased with an electric field of 60 kV cm^{-1} in each case. At this bias, the detuning of the corresponding injector and active

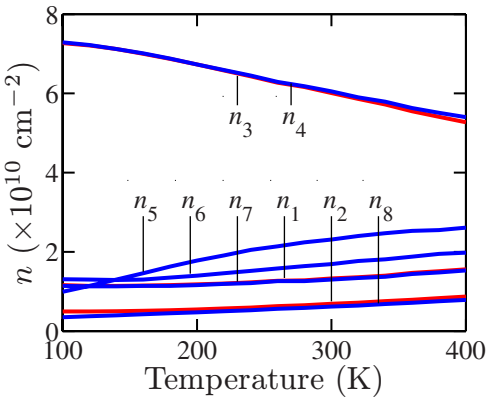

Figure 4. Carrier density at different levels versus temperature. The applied electric field is 60 kV cm^{-1}, and the total carrier density per period is 2×10^{11} cm^{-2}.

region levels is small. For example, the detuning of the injector ground level (level 4) and the upper lasing level (level 3) is only 0.5 meV. If coherence exists for a sufficiently long time, the carriers will oscillate between the two levels until they are equal. In figure 3(a), when $T = 100$ K, the carriers oscillate between the levels before settling down to a steady-state value due to significant coherent carrier transport and a slow decay of the coherence between the injector and active region levels. In this case, carrier injection into the active region and extraction from the active region are efficient. We note that the upper lasing level has nearly the same carrier density as does the injector ground level, i.e. $n_3 \approx n_4$. We also note that n_3 and n_4 are much greater than the carrier densities of other levels. Therefore, backscattering is less than that at higher temperatures. As the temperature increases further, the coherence time between the injector and active region levels diminishes. Therefore, fewer oscillations are visible in figures 3(b)–(d) and the density n_3 decreases. Even when the corresponding levels in the injector and active regions are close to resonance, coherent transport decreases as the temperature rises. We note that n_4 drops as electrons backscatter to upper energy levels, thereby further decreasing n_3. Therefore, the densities n_1, n_2, n_6, n_7 and n_8 increase as the temperature increases.

In figure 4, we show the steady-state carrier density at each level in the injector and active region as the temperature varies. The densities n_3 and n_4 decrease with temperature, while n_1, n_2, n_6, n_7 and n_8 increase as the temperature increases. These density changes are due to the decrease in the coherent carrier transport at a higher temperature and the increase in backscattering of electrons from levels 3 and 4 to the higher energy levels in the injector and the lower active region levels of the previous period.

We have calculated the coherence time between every injector level and every active region level as the temperature changes. The coherent transport between the injector ground level (level 4) and the upper lasing level (level 3) has the largest impact on the QCL performance. Hence, we plot the values of the coherence time between the injector ground level and the upper lasing level ($T_{2,34}$) versus temperature in figure 5 for three different total carrier densities per period. The coherence time monotonically decreases with temperature. However, the rate of decrease is larger at temperatures lower than 200 K. At temperatures greater than 400 K, we find that the temperature effects saturate. The coherence time also strongly depends on the total number of

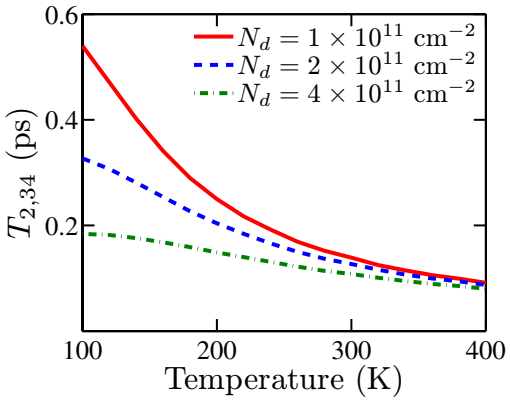

Figure 5. Coherence time between the upper lasing level (level 3) and the injector ground level (level 4) versus temperature. The applied electric field is 60 kV cm^{-1} and the total carrier density per period is 2×10^{11} cm^{-2}.

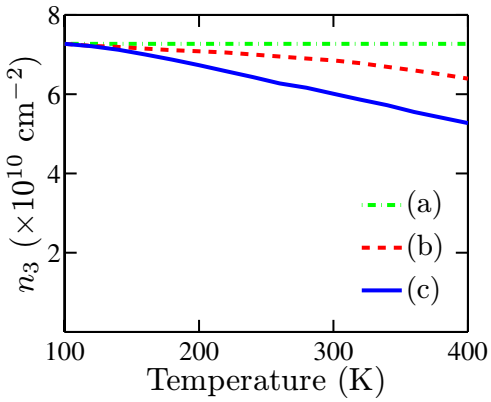

Figure 6. The upper lasing level carrier density for the cases when (a) both incoherent scattering processes and coherent tunneling are not allowed to vary as the temperature changes from 100 K, (b) only coherent tunneling is allowed to vary as the temperature changes from 100 K and (c) both incoherent scattering processes and coherent tunneling are allowed to vary as the temperature changes from 100 K. The applied electric field is 60 kV cm^{-1} and the total carrier density per period is 2×10^{11} cm^{-2}.

carriers in a period (N_d). The coherence time is 0.54 ps at 100 K with 1×10^{11} cm^{-2} carriers in one period, while it is only 0.18 ps at the same temperature with 4×10^{11} cm^{-2} carriers in one period.

The change in carrier densities in figures 3 and 4 as temperature changes is due to the temperature dependence of both incoherent scattering processes and coherent tunneling. Therefore, to determine the relative contribution of the temperature-dependent tunneling to the change in the carrier densities as temperature changes, we keep the rates of the incoherent scattering processes fixed at their values at 100 K and we allow only coherent tunneling to vary as temperature changes from 100 K. We plot the upper lasing level population as temperature changes for different cases in figure 6. From figure 6, it is evident that the temperature dependence of coherent tunneling plays a significant role in the carrier transport of QCLs.

4. Conclusions

In conclusion, we have studied the temperature dependence of the coherent carrier transport, i.e. carrier injection into an active region and extraction from an active region, of QCLs. We have shown that carrier injection and extraction decrease as the temperature increases, due to a decrease in coherence time. We note that several other effects can lead to a decrease in carrier injection and extraction as the temperature rises. These effects include thermal back-filling, leaking to the continuum and temperature dependence of the upper lasing level lifetime. The relative importance of carrier transport—and therefore its impact as the temperature increases—depends on the operating conditions, including the applied bias and the quantum mechanical design. We explicitly demonstrated for a realistic structure that this effect is important relative to incoherent scattering processes.

Coherent phenomena play an important role in the efficient transport of a carrier through a QCL, and it is usually desirable to maximize the carrier transport. Because the modeling approach we are using here is sufficiently powerful to capture coherent phenomena, while at the same time being sufficiently efficient computationally to model realistic structures, this modeling approach should become a conventional tool when designing QCLs.

In this analysis, we have assumed that the lattice and electrons of the QCL have the same temperature. In practice, the lattice and electrons will have different temperatures with an electron temperature that is always greater than the lattice temperature. The electron temperature can be significantly higher than the lattice temperature for continuous wave and high-power operation of the laser. Therefore, the phenomena discussed here should be observed at a lower lattice temperature. The values of the coherence time estimated in this work are somewhat large. We have calculated the coherence time by including all possible electron–LO-phonon scattering, electron–interface roughness scattering and dominant $x, x \rightarrow x, x$ and $y, y \rightarrow y, y$ electron–electron scattering. There are other scattering mechanisms such as $x, y \rightarrow x, y$ electron–electron scattering, electron–acoustic phonon scattering and electron–impurity scattering that, if included in the model, would slightly decrease the calculated coherence times. However, this decrease is not significant.

Acknowledgments

We gratefully acknowledge support from the MIRTHE Engineering Research Foundation, which is sponsored by the National Science Foundation. We thank Professors F-S Choa, C Gmachl, A Johnson and J Khurgin for useful comments.

References

[1] Sirtori C, Capasso F, Faist J, Hutchinson A, Sivco D and Cho A 1998 Resonant tunneling in quantum cascade lasers *IEEE J. Quantum Electron.* **34** 1722

[2] Choi H, Diehl L, Wu Z-K, Giovannini M, Faist J, Capasso F and Norris T B 2008 Gain recovery dynamics and photon-driven transport in quantum cascade lasers *Phys. Rev. Lett.* **100** 167401

[3] Eickemeyer F, Reimann K, Woerner M and Elsaesser T 2002 Ultrafast coherent electron transport in semiconductor quantum cascade structures *Phys. Rev. Lett.* **89** 047402

[4] Choi H, Norris T B, Gresch T, Giovannini M, Faist J, Diehl L and Capasso F 2008 Femtosecond dynamics of resonant tunneling and superlattice relaxation in quantum cascade lasers *Appl. Phys. Lett.* **92** 122114

[5] Wacker A 2008 Coherence and spatial resolution of transport in quantum cascade lasers *Phys. Status Solidi* **5** 215
[6] Razeghi M, Slivken S, Bai Y, Gokden B and Darvish S R 2009 High power quantum cascade lasers *New J. Phys.* **11** 125017
[7] Faist J, Capasso F, Sirtori C and Sivco D L 2000 *Quantum Cacade Lasers, Intersubband Transitions in Quantum Wells: Physics and Device Applications II* ed H C Liu and F Capasso (San Diego, CA: Academic)
[8] Faist J, Capasso F, Sirtori C, Sivco D L, Hutchinson A L and Cho A Y 1995 Vertical transition quantum cascade laser with Bragg confined excited state *Appl. Phys. Lett.* **66** 538
[9] Lyakh A *et al* 2008 1.6 W high wall plug efficiency, continuous-wave room temperature quantum cascade laser emitting at 4.6 μm *Appl. Phys. Lett.* **92** 111110
[10] Bai Y, Slivken S, Darvish S R and Razeghi M 2008 Room temperature continuous wave operation of quantum cascade lasers with 12.5% wall plug efficiency *Appl. Phys. Lett.* **93** 021103
[11] Semtsiv M P, Dressler S and Masselink W T 2007 Short-wavelength ($\lambda \approx 3.6\,\mu$m) $In_{0.73}Ga_{0.27}As$–AlAs–InP quantum-cascade lasers *IEEE J. Quantum Electron.* **43** 42
[12] Terazzi R and Faist J 2010 A density matrix model of transport and radiation in quantum cascade lasers *New J. Phys.* **12** 033045
[13] Kubis T, Yeh C and Vogl P 2008 Quantum theory of transport and optical gain in quantum cascade lasers *Phys. Status Solidi* **5** 232
[14] Jirauschek C 2010 Monte Carlo study of carrier–light coupling in terahertz quantum cascade lasers *Appl. Phys. Lett.* **96** 011103
[15] Indjin D, Harrison P, Kelsall R W and Ikonić Z 2002 Self-consistent scattering theory of transport and output characteristics of quantum cascade lasers *J. Appl. Phys.* **91** 9019
[16] Iotti R C and Rossi F 2001 Nature of charge transport in quantum-cascade lasers *Phys. Rev. Lett.* **87** 146603
[17] Iotti R C and Rossi F 2000 Microscopic theory of hot-carrier relaxation in semiconductor-based quantum-cascade lasers *Appl. Phys. Lett.* **76** 2265
[18] Donovan K, Harrison P and Kelsall R W 2001 Self-consistent solutions to the intersubband rate equations in quantum cascade lasers: analysis of a GaAs/$Al_xGa_{1-x}As$ device *J. Appl. Phys.* **89** 3084
[19] Nelander R, Wacker A, Pereira M F Jr, Revin D G, Soulby M R, Wilson L R, Cockburn J W, Krysa A B, Roberts J S and Airey R J 2007 Fingerprints of spatial charge transfer in quantum cascade lasers *J. Appl. Phys.* **102** 113104
[20] Savić I, Vukmirović N, Ikonić Z, Indjin D, Kelsall R W, Harrison P and Milanović V 2007 Density matrix theory of transport and gain in quantum cascade lasers in a magnetic field *Phys. Rev.* B **76** 165310
[21] Pereira M F Jr, Lee S-C and Wacker A 2004 Controlling many-body effects in the midinfrared gain and terahertz absorption *Phys. Rev.* B **69** 205310
[22] Talukder M A 2010 Analysis of self-induced transparency modelocking of quantum cascade lasers *PhD Dissertation* Department of Computer Science and Electrical Engineering, UMBC
[23] Ferreira R and Bastard G 1989 Evaluation of some scattering times for electrons in unbiased and biased single- and multiple-quantum-well structures *Phys. Rev.* B **40** 1074
[24] Hartig M, Haacke S, Deveaud B and Rota L 1996 Femtosecond luminescence measurements of the intersubband scattering rate in $Al_xGa_{1-x}As$/GaAs quantum wells under selective excitation *Phys. Rev.* B **54** 14269
[25] Harrison P 1999 The nature of the electron distribution functions in quantum cascade lasers *Appl. Phys. Lett.* **75** 2800
[26] Capasso F, Mohammed K and Cho A Y 1986 Resonant tunneling through double barriers, perpendicular quantum transport phenomena in superlattices and their device applications *IEEE J. Quantum Electron.* **22** 1853
[27] Luryi S 1989 Coherent versus incoherent resonant tunneling and implications for fast devices *Superlattices Microstruct.* **5** 375

[28] Barbieri S, Sirtori C, Page H, Stellmacher M and Nagle J 2001 Design strategies for GaAs-based unipolar lasers: optimum injector-active region coupling via resonant tunneling *Appl. Phys. Lett.* **78** 282

[29] Woerner M, Reimann K and Elsaesser T 2004 Coherent charge transport in semiconductor quantum cascade structures *J. Phys.: Condens. Matter* **16** R25

[30] Wittmann A, Bonetti Y, Faist J, Gini E and Giovannini M 2008 Intersubband linewidths in quantum cascade laser designs *Appl. Phys. Lett.* **93** 141103

[31] Lee S-C, Galbraith I and Pidgeon C R 1995 Influence of electron temperature and carrier concentration on electron–LO-phonon intersubband scattering in wide GaAs/$Al_xGa_{1-x}As$ quantum wells *Phys. Rev.* B **52** 1874

[32] Unuma T, Yoshita M, Noda T, Sakaki H and Akiyama H 2003 Intersubband absorption linewidth in GaAs quantum wells due to scattering by interface roughness, phonons, alloy disorder and impurities *J. Appl. Phys.* **93** 1586

[33] Smet J H, Fonstad C G and Hu Q 1996 Intrawell and interwell intersubband transitions in multiple quantum wells for far-infrared sources *J. Appl. Phys.* **79** 9305

[34] Sirtori C, Kruck P, Barbieri S, Collot P and Nagle J 1998 GaAs/$Al_xGa_{1-x}As$ quantum cascade lasers *Appl. Phys. Lett.* **73** 3486

[35] Liu Z, Wasserman D, Howard S, Hoffman A, Gmachl C, Wang X, T-Ek T, Cheng L and Choa F-S 2006 Room-temperature continuous-wave quantum cascade lasers grown by MOCVD without lateral regrowth *IEEE Photonics Technol. Lett.* **18** 1347